Laser-induced chemical transformation of graphene oxide – iron oxide nanoparticles composites deposited on polymer substrates

Angel Pérez del Pino,[a,*] Eniko György,[a,b] Constantin Logofatu,[c] Josep Puigmartí-Luis,[d] Wei Gao[e,f]

[a]Instituto de Ciencia de Materiales de Barcelona, Consejo Superior de Investigaciones Científicas (ICMAB-CSIC), Campus UAB, 08193 Bellaterra, Spain

[b]National Institute for Lasers, Plasma and Radiation Physics, P. O. Box MG 36, 77125 Bucharest, Romania

[c]National Institute for Materials Physics, P. O. Box MG. 7, 77125 Bucharest, Romania

[d]Swiss Federal Laboratories for Materials Science and Technology, Lerchenfeldstr 5, CH-9014, St. Gallen, Switzerland

[e]Textile Engineering, Chemistry and Science Department, North Carolina State University, Raleigh, NC, 27695, USA

[f]The Center for Integrated Nanotecnologies, Los Alamos National Laboratory, P.O. Box 1663, MS K771, Los Alamos, NM 87545, USA

Abstract

Ultraviolet laser irradiation of films composed of graphene oxide (GO) and GO-magnetite (Fe_3O_4) nanoparticles deposited on polydimethylsiloxane substrates is carried
Corresponding author. Tel: +34 935801853. E-mail: aperez@icmab.es (Angel Perez)

out. The irradiations are performed in vacuum and ammonia-rich gas environments. Electron and scanning probe microscopies reveal a rippling process in GO sheets as the accumulation of laser pulses proceeds, being the effect more pronounced with the increase of laser fluence. X-ray photoelectron spectroscopy analyses point to laser-induced chemical reaction pathways in GO completely different depending on the environment and the presence or absence of Fe_3O_4 nanoparticles. It is demonstrated that GO-based films with diverse type of oxygen- and nitrogen-containing chemical groups can be obtained by means of laser irradiation processes. The sheet resistance of these materials is also correlated to their structure and composition.

1. Introduction

Graphene oxide (GO) has become a material of great value due to its fascinating physicochemical properties [1-3] and to its ability to be transformed into a graphene-like material, called reduced graphene oxide (rGO). This deoxygenating process can be obtained in large-scale and in an exceptionally cost-effective manner. Besides, composite materials based on graphene/rGO and metal oxide nanostructures have emerged as a subject of enormous scientific interest due to their high potential impact in diverse technological areas [4-6]. Particularly, graphene- and rGO-Fe_3O_4 nanohybrids are very promising to be used as active materials in strong electromagnetic interference attenuation systems [7,8], chemical sensors [9,10] as well as in energy storage devices such as lithium ion batteries and supercapacitors [11,12], among others. It is worth noting that most of these high performance devices are preferred to be lightweight and conformable in order to be used in diverse types of systems [12,13]. Thus, the support of rGO-Fe_3O_4 composites on polymer substrates is desirable. Recent works point to the

improvement of rGO and rGO-Fe_3O_4 materials' functional properties, such as oxygen reduction reaction yield and supercapacitor performance, after the nitrogen doping of the graphene structure [14-16] due to the modulation of optical and electronic properties [17]. Particularly, doping of graphene structure by graphitic (substitutional) nitrogen provokes a n-type behaviour, whereas pyridinic and pyrrolic N may lead to a p-type performance, instead. Thus, an easy and versatile method for synthesizing N-doped graphene-based materials is driving great research interest.

The fabrication of rGO-Fe_3O_4 hybrid materials is typically achieved by complex chemical methods many of them involving high temperature processes [18,19] which cannot be compatible with polymer substrates. Moreover, most of the synthesis procedures usually use toxic and/or hazardous agents. Thus, it is necessary to develop environment-friendly methods for the preparation of these types of materials. Conversely, laser irradiation techniques have recently emerged as versatile, scalable, eco-friendly and easy ways for fabricating thin films composed of rGO-metal oxide nanostructures either by direct irradiation [20] or laser deposition [21,22] methods. Remarkably, the nature of ultraviolet pulsed laser radiation could lead to the attainment of new chemical pathways for the development of graphene-based nanocomposites with improved functionalities to be used in future devices. To the best of our knowledge, no works regarding the laser treatment of GO-Fe_3O_4 hybrids exist in the scientific literature.

We present the easy fabrication and characterization of rGO and rGO-Fe_3O_4 nanoparticles (NPs) composite films on polydimethylsiloxane (PDMS) substrates from their oxidized form (i.e. GO and GO-Fe_3O_4 composite films) by means of nanosecond pulsed UV laser irradiation. Though, in principle, any polymer can be used as substrate PDMS has been chosen due to its optical transparency, ease of functionalization as well

as inert, non-toxic, and heat stability properties [23]. The experiments are done in vacuum and under ammonia-rich atmosphere conditions, which enables the reduction and nitrogen doping of the generated GO structures. Comparative studies of the morphology, chemical composition and sheet resistance of the irradiated GO/PDMS and GO-Fe_3O_4/PDMS composite films are shown, indicating a rich chemical phenomenology which depends on laser parameters and the chemical environment.

2. Experimental

Two types of dispersions were prepared for the synthesis of GO and GO-Fe_3O_4 nanocomposite films. The solutions respectively consisted of (i) 0.5 wt. % GO plates (sheets around 1 μm^2 area, provided by Nanoinnova Technologies), and (ii) 0.05 wt. % Fe_3O_4 NPs (about 50-100 nm in size, Sigma-Aldrich) and 0.5 wt. % GO plates, all of them dispersed in distilled water. The weight percentages used in this work ensure the mechanical stability and adhesion of the deposited films on PDMS, in addition to a moderate electrical conductivity provided the insulating nature of Fe_3O_4 NPs. The PDMS membrane used as substrate in our experiments was prepared pouring a mixture of PDMS oligomer and cross-linking agent (hardener) 10 to 1 in weight inside a plastic petri dish. The PDMS and the cross-linking agent were purchased from Dow Corning (SYLGARD® 184 Silicone elastomer kit). In order to ensure a flat and smooth PDMS substrate the mixture was cured at room temperature in a level surface during 24 hours. After that, the cured PDMS substrate was peeled off from the plastic petri dish and cut with a razor blade in small pieces of 10×10 mm^2 and about 1 mm in thickness. Next, in order to ensure a good film formation on top of the PDMS membrane, the PDMS pieces were plasma treated in air with a corona discharge during 2 minutes (Electro Technic

Products, INC.) and subsequently placed under a pressurized chamber containing N-[3-(trimethoxysilyl)propyl]-ethylenediamine (TPEDA, Sigma-Aldrich, 97%) vapours. This treatment with TPEDA vapours was conducted during 12 hours and facilitated the formation of amine groups on the PDMS substrate that favour a well spread film formation. The pressure was regulated to be around 0.5−0.8 bars during the treatment. Subsequently, 200 μL of the synthesized graphene oxide-based dispersions, previously sonicated during 1 h, were casted on functionalized PDMS substrates. GO/PDMS and GO-Fe_3O_4/PDMS samples were respectively heated at 100ºC and 50°C until they dried. This methodology ensured a regular, unbroken and uniform film formation with thickness in the micron range.

The obtained samples were exposed to a laser irradiation process at room temperature inside a reaction chamber, which was previously evacuated down to a residual pressure of 10^{-4} Pa. Irradiation experiments were made using a Nd:YAG (λ = 266 nm, τ_{FWHM} = 3 ns, ν = 10 Hz) laser system (Brilliant model from Quantel), applying 10, 100 and 1000 subsequent laser pulses with an incident laser fluence of 40 and 100 mJ cm^{-2}. A squared laser spot, 1×1 mm^2 in size, and highly homogeneous intensity distribution was used by means of a beam homogenizer and mask system. The irradiations were performed in vacuum (at residual pressure), or in ammonia (NH_3)-rich environment at nearby atmospheric pressure. In this last case, the NH_3–rich environment was obtained by flowing N_2 gas through an ammonia solution (30% v/v) and introducing the gas mixture in the reaction chamber. Non-irradiated reference drop-cast thin films (raw) were also prepared from initial dispersions for comparison to the laser treated ones.

Numerical simulations were carried out in order to obtain a general view of the laser-induced temperature evolution in simple GO and GO-Fe_3O_4 NPs systems (model

described in Supporting Information). The calculations were done solving the two-dimensional heat equation in compact GO/PDMS films (0.1 – 1 μm GO film thickness deposited on PDMS substrate) and in 50 nm-sized Fe_3O_4 NP on GO/PDMS systems by means of COMSOL 5.0 software. For the sake of simplicity, and the lack of knowledge about the fine arrangement of the raw material and their real physical properties, the model only contemplated photothermal mechanisms in an idealized system, neglecting the effects of nanometric dimensions on optical properties and heat transport. The optical and thermophysical properties of GO and Fe_3O_4, summarized in Table S1, were obtained from Refs. [24-27,*]. The morphology of the deposited films was studied by field emission scanning electron microscopy (SEM) with the aid of a QUANTA FEI 200 FEG-ESEM system. Secondary electrons images were acquired at 50 Pa background pressure. 3D analysis of the surface morphology was investigated through atomic force microscopy by means of an Agilent 5500LS system working at intermittent contact mode. Compositional studies of the obtained materials were accomplished by X-ray photoelectron spectroscopy (XPS). The measurements were done using a SPECS XPS spectrometer based on Phoibos 150 electron energy analyzer which operated in constant energy mode. The Mg Kα line, centered at 1253.6 eV, was used for monochromatic X-ray excitation. High resolution spectra were acquired over ranges of 20 eV, at 10 eV pass energy and energy resolution of 0.7 eV. The analyses were made in a 10^{-7} Pa ultra-high vacuum environment. Finally, the electrical nature of the obtained thin films was studied by means of sheet resistance measurements in 1×1 mm^2 film areas using a micro-probe station equipped with tips with a diameter of 10 μm and with a Keithley 2612B source-meter system.

3. Results and Discussion

[*] www.engineeringtoolbox.com; COMSOL Materials Library.

Patterns and squared areas with different sizes were straightforwardly fabricated by laser irradiation of adjacent 1×1 mm^2 surface areas with high precision. Fig. 1a reveals that as deposited GO-based films display uniform grey colour and become black when irradiated. Thermal simulations in GO/PDMS and GO-Fe_3O_4/PDMS films are presented in Fig. 1b. Idealized systems consisting on GO/PDMS and Fe_3O_4 NPs on GO/PDMS were simulated. The calculations evidence that ultraviolet laser radiation is absorbed in both Fe_3O_4 NPs and GO leading to similar heating evolution independently on the films thickness in the range 100 nm – 1 μm. Thus, laser pulses provoke short thermal cycles up to 1 μs in duration, with fast heating intervals showing rates up to ~10^{12} K s^{-1} and much longer cooling times. The maximum calculated surface temperature in GO/PDMS films is about 1700 K and 3900 K when irradiated with 40 and 100 mJ cm^{-2}, respectively. Nonetheless, the real temperature may be lower due to the expected porosity present in GO films created by the randomly oriented deposition of GO flakes during the casting process. Besides, the maximum temperature reached in GO is below its theoretical melting point (4800 K). As seen in inset of Fig. 1b, the temperature abruptly drops across the film, caused by the rapid distribution of the thermal energy through the film material, and no thermally-induced damage of PDMS substrate may be done. This fact has been indeed verified by rear-side inspection of the film-PDMS interface which shows no alteration at all. On the other hand, 50 nm-sized Fe_3O_4 NP on GO/PDMS film shows faster temperature rising when laser irradiated mainly due to the much larger optical absorption coefficient of Fe_3O_4 than that of GO (Table S1). Fe_3O_4 NPs reach their melting temperature (1811 K) even after 40 mJ cm^{-2} irradiation, whereas they would even attain their vaporization point when irradiated with 100 mJ cm^{-2}.

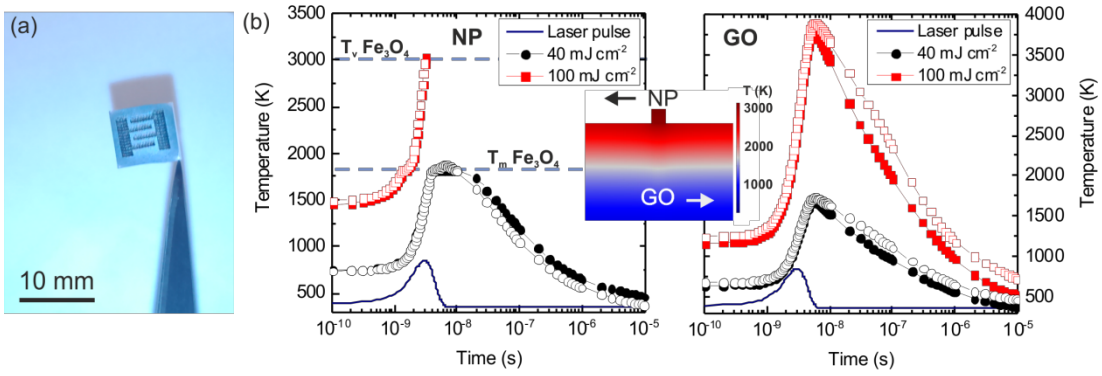

Fig. 1. (a) Image of irradiated pattern in GO/PDMS film. (b) Simulated surface temperature evolution of GO/PDMS and Fe_3O_4 NP on GO/PDMS films irradiated with one laser pulse at (●) 40 mJ cm^{-2} and (■) 100 mJ cm^{-2}. Solid and open symbols represent numerical calculations considering 100 nm and 1 μm in GO thickness, respectively. Laser pulse intensity time evolution in arbitrary units is also plotted for reference. Inset: temperature distribution in the GO-Fe_3O_4 NP system irradiated with 100 mJ cm^{-2} @ 3 ns.

Fig. 2 presents SEM images of the obtained samples. On the one hand, as deposited GO films (raw) totally cover the PDMS surface and are composed of overlapped GO flakes (Fig. 2a). The surfaces are smooth though reveal micron-sized protuberances and corrugations of few hundreds of nm in height, caused by bending of GO sheets during their assembly. The laser irradiation of GO/PDMS films leads to a similar surface morphology evolution independently of the gas environment employed during the experiments. Conversely, a clear distinction of the surface morphology is observed after the accumulation of laser pulses at different laser fluences, being the effects more profound at high fluence values. After the accumulation of low number of pulses with 40 mJ cm^{-2} fluence, the GO morphology is mainly unchanged though some locations

show the presence of irregularities and small filament-like features around 1-3 μm in length (Fig. 2b). The subsequent accumulation of laser pulses leads to the increase of the structures' extent. Laser irradiation with 100 mJ cm^{-2} leads to the formation of a rough morphology composed of larger filament structures even with just 10 pulses. An increase of the laser pulses leads to the formation of greater features and trenches, and after 1000 pulses, mountain-like structures with a few microns in size can be appreciated (Fig. 2c). The round aspect of the mountain-like structures would point to a substantial melting of the irradiated material and merging mechanisms as the mean cause of their formation. On the other hand, as deposited GO-Fe_3O_4/PDMS films show oxide NPs located on the smooth and wavy GO surfaces (Fig. 2d). The NPs, which have dimension in the range of 50 to 100 nm in diameter, form small aggregates which decorate the GO surface in a non-uniform way. Interestingly, the NPs do not build high aggregates but tend to form thin extended arrangement of aggregates, some of them showing a kind of aligned conformation (Figs. 2d and 3a). This effect could indicate a significant interaction degree between NPs and GO surfaces. After laser irradiation, NPs reveal a rounded shape and larger dimensions as compared to the initial material, thus indicating a melting process (Figs. 2e and f) which is indeed predicted by the numerical calculations (Fig. 1b). Coalescence between molten NPs prior their resolidification process would be also present, as already observed during irradiation of GO-ZnO NPs composites [20]. This effect is clearly witnessed after the accumulation of 1000 pulses with 40 mJ cm^{-2} fluence, but just after 10 pulses with 100 mJ cm^{-2}. However, no signs of Fe_3O_4 NPs vaporization are observed indicating that NPs' calculated temperatures are overestimated mainly due to the numerical model constraints during molten phase. As regards the GO flakes forming the GO-Fe_3O_4/PDMS nanocomposites, they evolve similarly to those contained in GO/PDMS films with the laser treatment (Figs. 2e and f).

AFM analyses, presented in Figs. 3b-d, reveal that initial laser processing with 40 mJ cm^{-2} fluence induces some rippling of GO sheets, about 10 nm in height, besides the formation of filament-like structures a few hundreds of nm long and up to 150 nm in height and width (Fig. 3b). Further accumulation of pulses provokes the development of larger filaments with dimensions up to 400 nm in height-width at 1000 pulses. As observed in AFM and SEM images, a large amount of filaments tend to align in parallel lamellas leading to the formation of bundle superstructures. Irradiation with 100 mJ cm^{-2} leads to the development of larger structures, being the mountain-like features mainly composed of parallel filaments (Figs. 3c and 3d). However, some of the mountain-like structures begin to show smoother surface after the accumulation of 1000 pulses, reaching up to 500 nm in height. The rounded and flat shape of the surface features could point to a significant melting of the material, even though the thermal calculations show that laser irradiation would not reach its melting point at any experimental conditions (Fig. 1b).

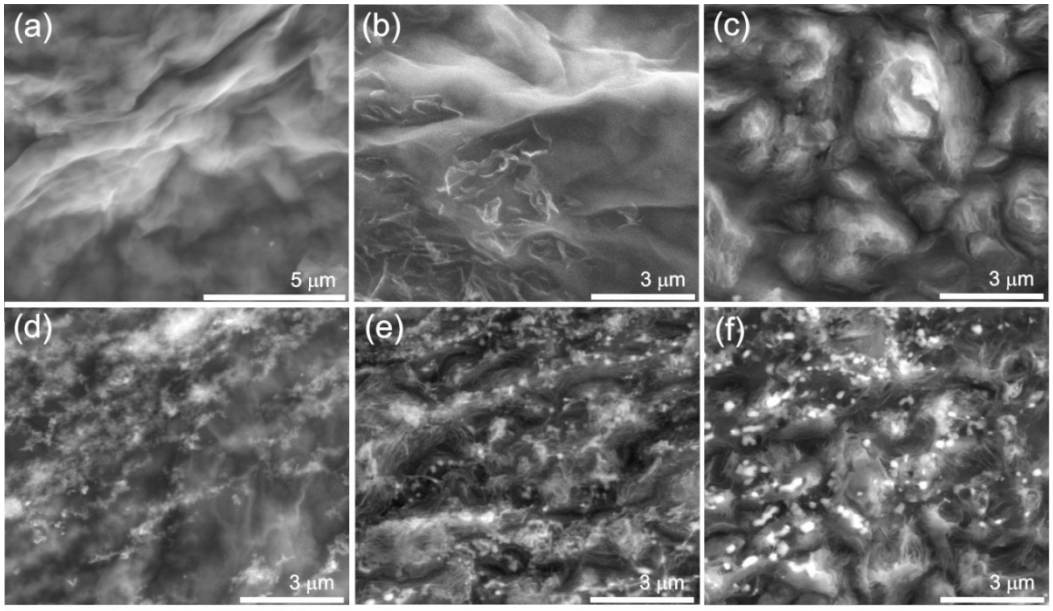

Fig. 2. Electron microscopy images of GO/PDMS films (a) as deposited, and irradiated in NH_3 ambient at (b) 40 mJ cm^{-2} accumulating 10 pulses, (c) 100 mJ cm^{-2} accumulating 1000 pulses, and GO-Fe_3O_4/PDMS films (d) as deposited, and irradiated in vacuum with 100 mJ cm^{-2} accumulating (e) 10 and (f) 1000 pulses.

Laser-induced development of ripple-like structures in GO material has been already reported [20,28]. UV radiation not only generates very rapid temperature variations in the material (Fig. 1b) but it can also prompt photochemical reactions which would induce chemical modification of the GO structure, as it will be revealed later. Then, the origin of the observed wrinkle to filament-like morphology evolution could be ascribed to the steady deformation of the GO sheets triggered by the creation of structural defects [29-31] and chemical functionalization [32]. Besides thermal fluctuations, the development of extremely high temperature gradients in reduced regions due to the presence of different intrinsic defect sites in GO sheet could significantly contribute to the formation of a stress-induced bending, the arrangement of the wrinkles and the formation of resonant features [33-35]. In a similar way, prominent corrugation of multiwall carbon nanotubes shells induced by UV laser radiation has been recently observed [36]. As the accumulation of pulses proceeds, the build-up and propagation of crystalline defects carries out. The sites with high enough density of crystalline defects and low dissociation energy chemical bonds, generated by previous laser pulses, would probably act as nucleation sites for local premelting processes at temperatures below that for “bulk” graphene [37]. Then, the accumulation of laser pulses would promote the concomitant melting to some extension of the graphene-based material as observed in samples processed with the maximum laser fluence and a high number of applied pulses (e.g. 1000 pulses).

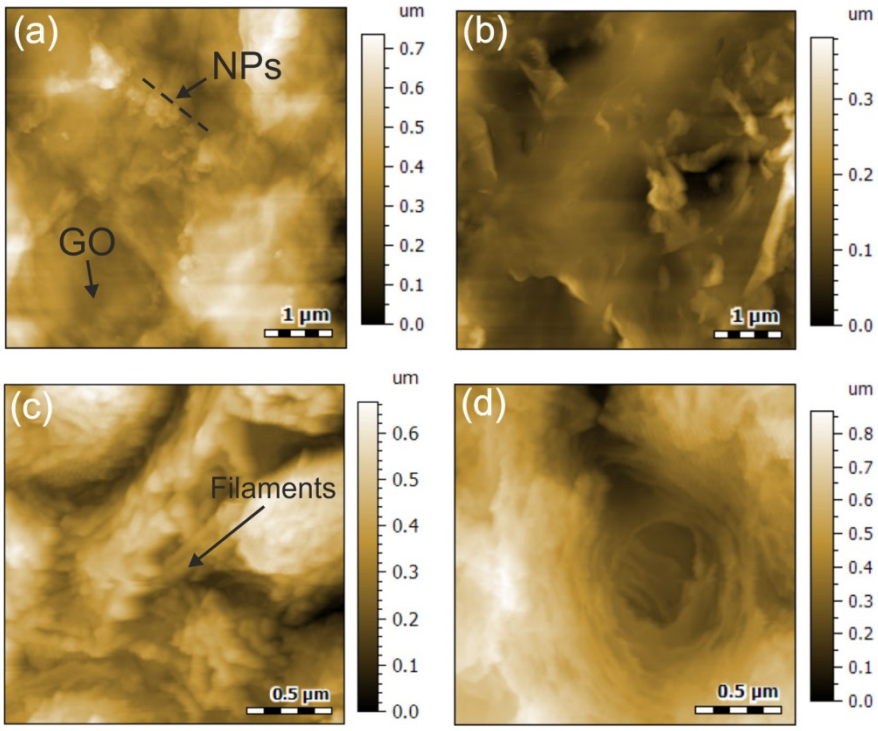

Fig. 3. AFM images of GO-Fe_3O_4/PDMS layers (a) as deposited, and irradiated with (b) 40 mJ cm^{-2} accumulating 100 pulses in vacuum, (c) 100 mJ cm^{-2} accumulating 100 pulses in NH_3 ambient, and (d) 100 mJ cm^{-2} accumulating 1000 pulses in vacuum.

XPS compositional analyses were carried out to freshly prepared samples, as well as to those subsequently treated with 100 mJ cm^{-2} laser fluence and after accumulation of 1000 pulses (Figs. 4 and 5). C1s spectra of GO/PDMS films were deconvoluted in four peaks CI, CII, CIII and CIV, centred at 285, 286, 287.5 and 289 eV, respectively. CI is ascribed to sp^2 graphitic carbon atoms, CII is attributed to carbon atoms having single bonds to oxygen atoms, i.e. epoxide (C-O-C) and hydroxyl (C-OH), whereas CIII and CIV are ascribed to carbon atoms having a double bond to oxygen atoms, carbonyl (C=O) and carboxyl (COOH) functional groups, respectively [38]. Fig. 6 presents the relative percentage of integrated peak areas in all the studied samples. As observed, C1s signal of deposited GO on PDMS (GO Raw) exhibits a large content of oxygen

functional groups since about 65% of the integrated area corresponds to carbon-oxygen components, CII (35%), CIII (25%) and CIV (5%), and just 35% to C=C graphitic signal. Moreover, N1s high resolution spectrum presents an asymmetric shape. This signal, which is relatively weak, was deconvoluted in two peak contributions, NI (~399.7 eV) and NII (~402.0 eV) respectively attributed to amine and pyridinic N^{+}-O^{-} groups (Fig. S1) [38], being the latter the most intense one (85% of integrated area). Therefore, the nature of GO raw material is mainly characterized by the presence of carbon-oxygen single-bonded groups in addition to a slightly lower content of double-bonded carbon-oxygen and carbon-nitrogen functionalities.

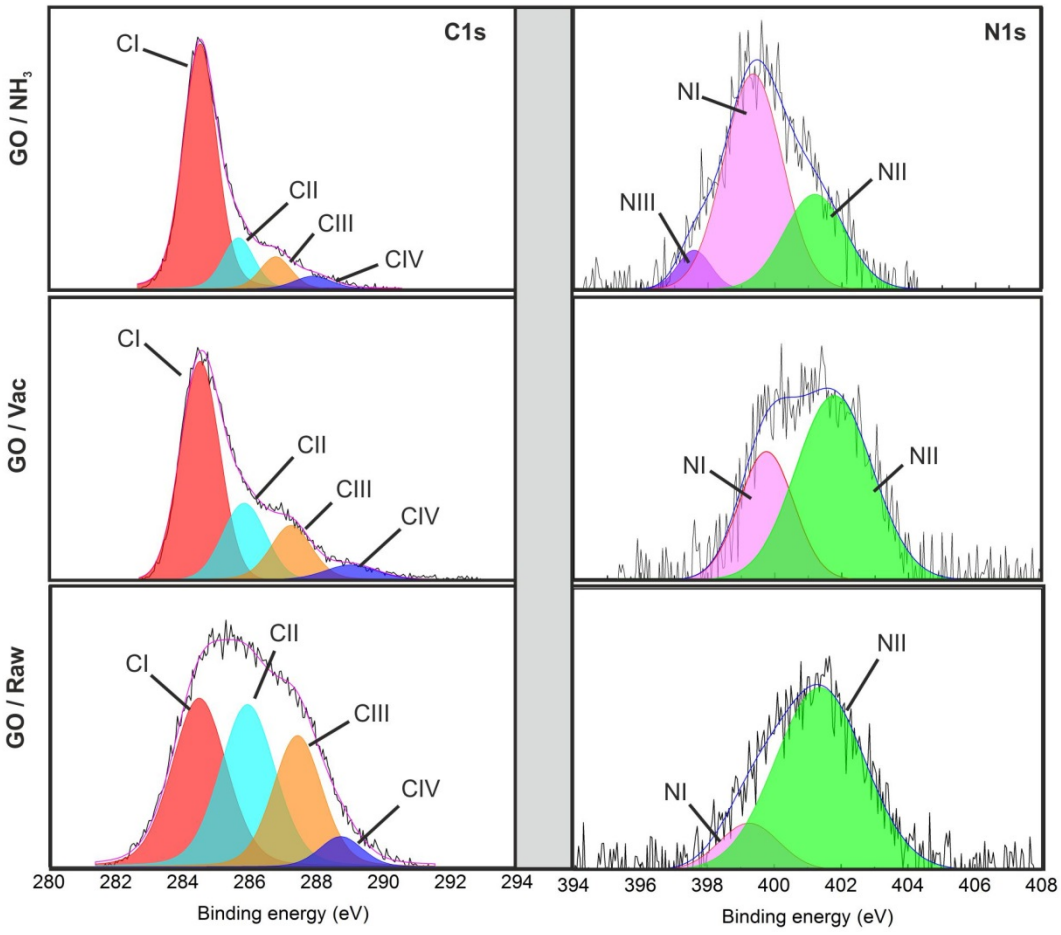

Fig. 4. High resolution C1s and N1s XPS spectra of GO layers as deposited on PDMS substrate (GO/Raw), and laser irradiated with 1000 accumulated pulses at 100 mJ cm^{-2} in vacuum (GO/Vac) and in NH_3 atmosphere (GO/NH_3).

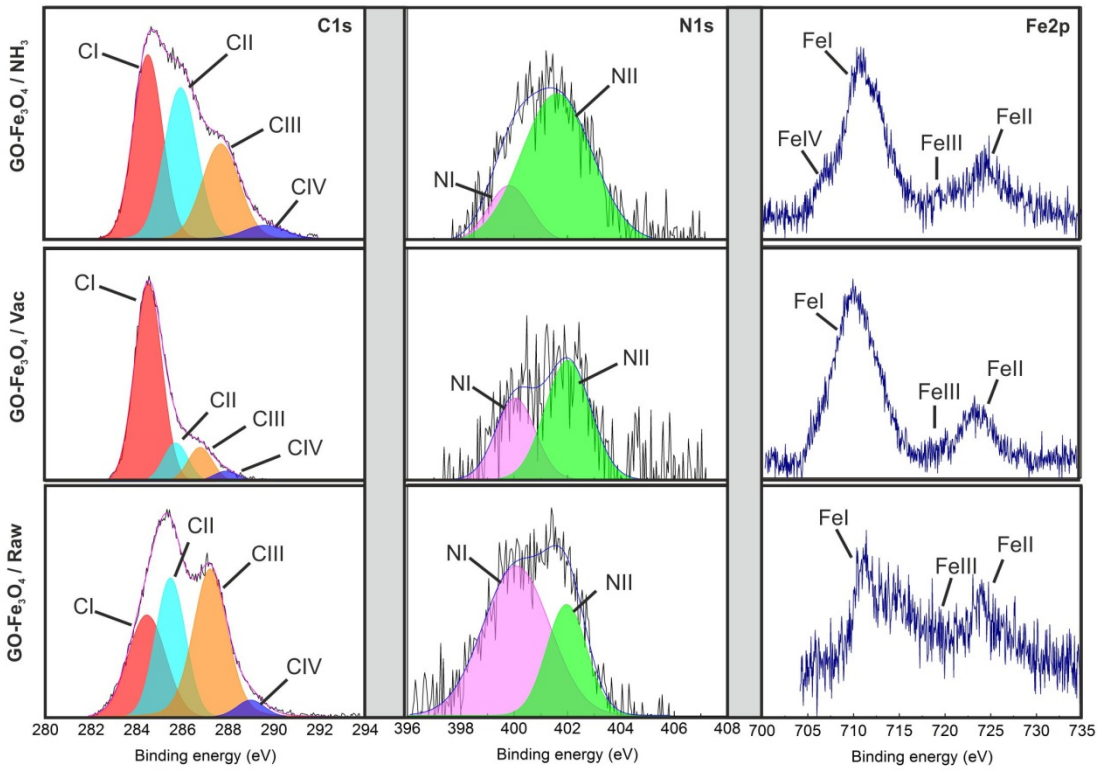

Fig. 5. High resolution C1s, N1s and Fe2p XPS spectra of GO-Fe_3O_4/PDMS films as deposited (GO-Fe_3O_4/Raw), and irradiated with 100 mJ cm^{-2} accumulating 1000 pulses in vacuum (GO-Fe_3O_4/Vac) and in NH_3 ambient (GO-Fe_3O_4/NH_3).

Fig. 7a shows a scheme of GO raw structure. Laser irradiation of GO/PDMS films in vacuum environment leads to the relative increase of CI peak, and the lowering of CII and CIII contributions. CIV peak practically remains unchanged. Thus, C=C graphene signal corresponds to around 57%, single-bonded carbon-oxygen and carbonyl groups signals respectively decrease to ~22% and ~16%, whereas the signal from carboxyl

groups marginally increases to 6%. Accordingly, not only a partial photoreduction of GO material is obtained, but also this mechanism is revealed to be much more effective in case of the hydroxyl-epoxide-carbonyl groups as compared to the carboxyl ones. Reported studies on GO photoreduction mechanisms reveal a complex evolution of migration and transformation mechanisms of the chemical species [39]. The activation energies for the photo-induced migration of hydroxyl groups and for the initiation of chemical reactions of multiple functional groups are below 0.5 eV. Hydroxyl photolysis and migration of ether oxygen atoms require less than 1 eV energy, whereas the complete reduction and photolysis of the rest of oxygen-containing groups requires higher energies. As revealed by thermal simulations, laser radiation induces a rapid heating of the GO material which, besides photochemical mechanisms, would provide enough energy to prompt the photolysis of hydroxyl, epoxide and carbonyl assemblies. Carboxyl moieties would mainly remain more stable during the irradiation process. The prolonged irradiation would lead to the elimination of larger amount of chemical groups as well as a probable photo-fragmentation of graphene backbone into molecular species [39], what would account for the observed GO morphology evolution (Figs. 2 and 3). Additionally, the laser-induced structural defects created in rGO flakes, which are highly reactive, could significantly contribute to the conversion of chemical groups [40]. On the other hand, N1s spectrum measured in GO irradiated in vacuum reveals lower content of nitrogen with a higher decomposition yield of pyridinic N-O than amine groups since NII integrated area decreased to about 67%. As expected, irradiation of GO/PDMS films in NH_3-rich ambient produces a different chemical pathway. As observed in C1s signal (GO / NH_3 in Figs. 4 and 6), an enhanced reduction of GO is taking place, since CI peak reaches ~73% of the integrated area, whereas (CII, CIII) peaks area represents (~14%, ~9%) which are lower than those obtained in vacuum

conditions. Moreover, CIV peak contribution decreases to about ~4% revealing that, in this case, a noteworthy photolysis of all the functional groups is carried out. This result clearly evidences that under ammonia environment conditions the yield of photolysis processes, and hence of reduction chemical processes is greater. Remarkably, nitrogen XPS spectrum is characterized by the significant augment of amine signal (64% of integrated area) and the appearance of NIII peak at ~398.6 eV, attributed to pyridinic nitrogen in graphene structure (Fig. S1) [41], which contributes with 7% of the integrated area. A sketch of the described structure is shown in Fig. 7b. It should be noted that pyridinic N-C atomic configuration would also contribute to CII peak, decreasing the relative content of hydroxyl-epoxide groups to this signal. It is recently reported that low temperature annealed GO material in ammonia environment leads to the formation of amine groups which, after higher temperature processing and in combination to oxygenated chemical groups, are transformed to basal pyridinic nitrogen moieties [42]. Pyridinic nitrogen sites, more specifically their nearly carbon atoms, play an essential role in oxidation-reduction reaction (ORR) processes [43] which add high value to N-doped graphene as functional material. Furthermore, partially reduced GO containing nitrogen-species (as amino and amide groups) would exhibit simultaneous p- and n-type semiconducting nature, being an effective photocatalytic medium for overall water decomposition into H_2 and O_2 with improved efficiency at visible wavelengths [14,44]. Thus, UV laser irradiation of GO/PDMS films under NH_3 ambient conditions emerges as a versatile method for the development of such type of systems.

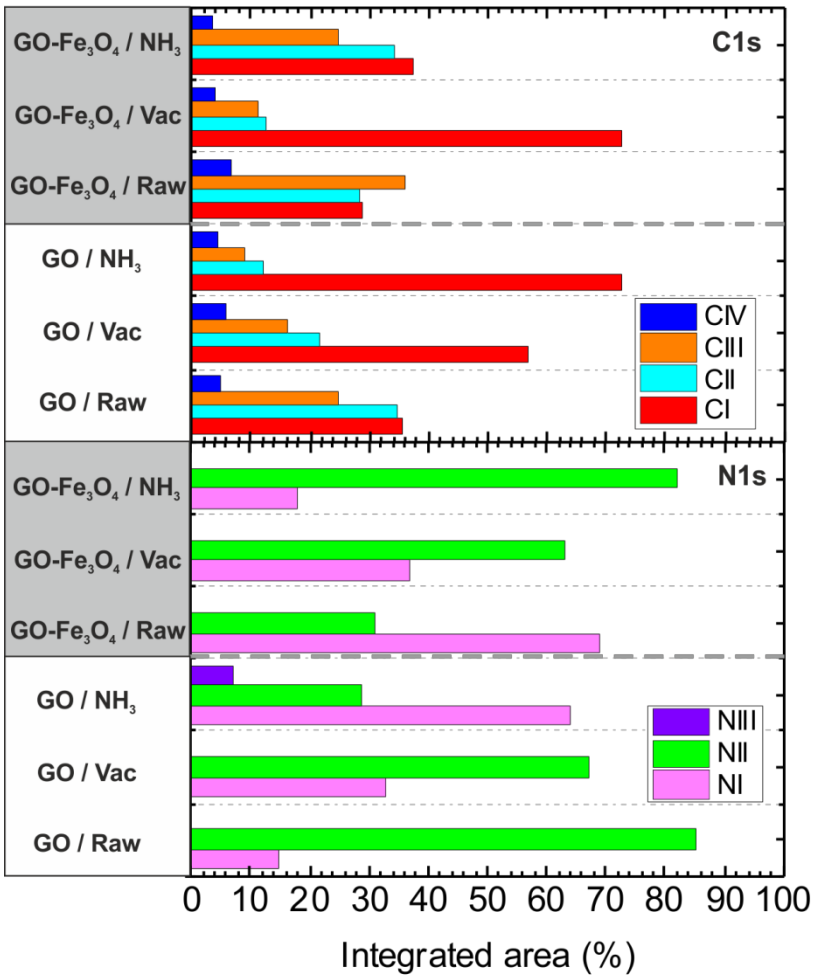

Fig. 6. Integrated area of XPS C1s and N1s deconvoluted peaks of GO/PDMS and GO-Fe_3O_4/PDMS films as deposited and irradiated with 1000 pulses at 100 mJ cm^{-2} in vacuum and in NH_3 environment.

XPS characterization of GO-Fe_3O_4/PDMS films reveals a completely different chemical evolution caused by the presence of Fe_3O_4 NPs (Fig. 5). First of all, C1s spectrum of as deposited GO-Fe_3O_4/PDMS films reveals an oxidized nature as compared to GO/PDMS raw material (see CII, CIII and CIV lines intensities for GO/Raw and GO-Fe_3O_4/Raw in Fig. 6). CI signal represents about 29% of the integrated area, whereas CII, CIII and CIV account for 28%, 36% and 7%, respectively in case of the GO-Fe_3O_4 film. Let us

recall that (CI, CII, CIII, CIV) integrated area values in GO raw material are (36%, 35%, 25%, 5%). Therefore, the significant decrease of CI and CII, and the augment of CIII and CIV signals indicate that the Fe_3O_4 NPs would mainly promote the catalytic decomposition of hydroxyl and epoxide groups in addition to a partial transformation to carbonyl and carboxyl groups. This effect is supported by the fact that Fe_3O_4 NPs are known to exhibit active catalytic performance in ORR processes [45-47]. Additionally, deconvoluted N1s spectrum of raw GO-Fe_3O_4/PDMS shows a major contribution of NI (amine) rather than NII (pyridinic N^+-O^-) signals with respective contributions to integrated area of 69% and 31%. This configuration is different to that observed in raw GO/PDMS films, where pyridinic N-O signal prevails, and it would be also supported by the known activity of Fe_3O_4 material in nitrogen-containing chemical reactions [48]. Regarding the composition of the oxide nanoparticles, Fe2p XPS spectrum was recorded, mainly revealing two weak peaks FeI and FeII, located at ~711 eV and ~724 eV, respectively. FeI peak is attributed to Fe $2p_{3/2}$ (4-fold degeneracy) whereas FeII is ascribed to Fe $2p_{1/2}$ (2-fold degeneracy) states. The Fe $2p_{3/2}$ peak appears to be noticeably asymmetric and the contribution of a very weak satellite (FeIII), located at around 717-719 eV, can be perceived indicating the presence of Fe_2O_3 (transformation of some Fe^{+2} ions to Fe^{+3}) [49]. Summarizing, GO-Fe_3O_4/PDMS are probably composed of Fe_3O_4-Fe_2O_3 NPs decorating oxidized GO sheets, with larger ratio of carbonyl-carboxyl groups over hydroxyl-epoxide ones, and amine over pyridinic N-O groups than raw GO material. A sketch of the structure is shown in Fig. 7c. As expected, laser irradiation of these films in vacuum environment increases the CI signal (~72%) and decreases that of CII (~13%), CIII (~11%) and CIV (~4%) ones when compared to raw GO-Fe_3O_4/PDMS samples. Therefore, during irradiation under vacuum conditions, oxygen-containing groups are efficiently removed leading to a

significant increase of the ratio of graphitic to oxygen containing carbon bonds. This deoxygenation effect is larger than that obtained in GO/PDMS irradiated in the same conditions. The Fe2p spectrum mainly reflects FeI and FeII peaks, showing higher intensity probably due to the enlargement of oxide NPs after irradiation (melting-coalescence-solidification). Further, FeI peak shows a more symmetric shape and FeIII peak is practically insignificant, pointing to the possible transformation of Fe_2O_3 to Fe_3O_4 materials (Fe^{+3} to Fe^{+2}) [49]. These results suggest that, whereas some oxygen seems to incorporate to GO and oxide NPs forming Fe_2O_3 during the GO-Fe_3O_4 NPs mixing and film deposition, laser irradiation in vacuum facilitates the inverse process leading to both the back transformation of Fe_2O_3 to Fe_3O_4 material and reduction of GO sheets. On the other hand, N1s spectrum reveals that this type of laser treatment produces the decrease of the amine signal (~37%) related to pyridinic N-O (~63%) contrarily to similar irradiation procedure applied to GO/PDMS films. Finally, laser irradiation of GO-Fe_3O_4/PDMS films in NH_3-rich ambient also reveals a different composition evolution than GO/PDMS films. In this case, CI, CII and NII signals increase as compared to as deposited GO-Fe_3O_4/PDMS films, being their respective integrated area ~37%, ~34% and ~82%. In lieu, CIII, CIV and NI signals decrease their contribution to ~25%, ~4% and ~18% of integrated area, respectively. No signs of pyridinic nitrogen are visible as in GO/PDMS films irradiated in analogous experimental conditions. Instead, NII peak intensity increase could be ascribed to the augment of pyridinic N-O groups and to the formation of quaternary nitrogen in the graphene structure [42]. In this case, additional C-N bonds should be endorsed to CII signal, which would indeed contribute to its observed increase. The overall Fe2p spectrum can be recognized as the typical of Fe_3O_4 material, showing intense FeI and FeII peaks, and almost no signal related to FeIII. However, FeI peak shows a shoulder

located at about 707 eV (FeIV) which is attributed to metallic iron (Fe^0) [50]. Consequently, laser treatment of GO-Fe_3O_4/PDMS in NH_3 environment provokes a moderate reduction of GO sheets mainly removing carbonyl and carboxyl groups, besides the creation of some hydroxyl-epoxide groups in addition to pyridinic N-O and, probably, graphitic N. The active species taking place in this reaction would be mainly provided by the functional groups from GO, and the NH_3-N_2-H_2O gas mixture, but also from oxide NPs material since its partial reduction to Fe^0 has been observed.

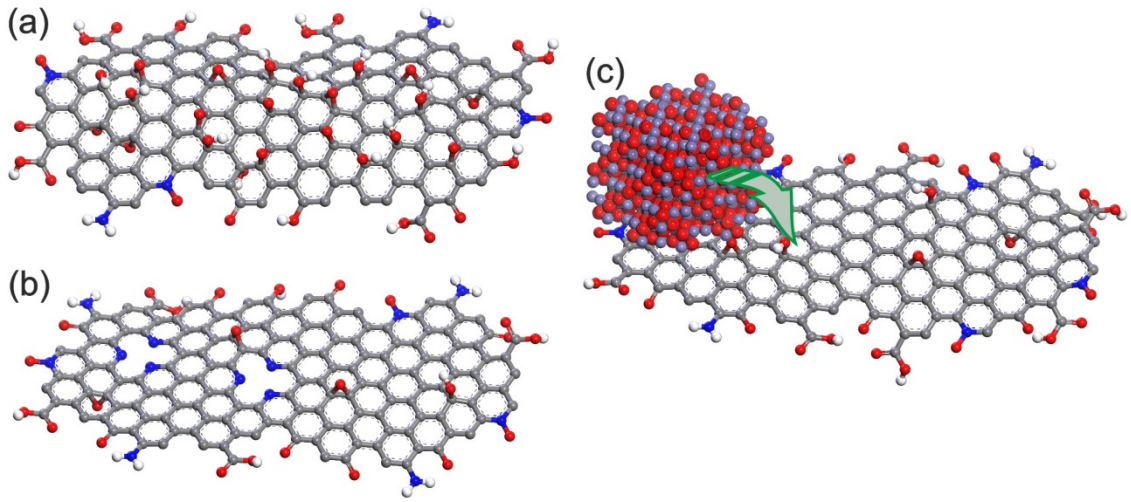

Fig. 7. Schematic illustration of the chemical structure of GO, according to the Lerf-Klinowski model, in (a) raw material, (b) when laser irradiated in NH_3 ambient, and (c) GO-Fe_3O_4 raw material. Atom colour: ● Fe, ● C, ● N, ● O, ○ H.

Topographic and compositional nature of GO/PDMS and GO-Fe_3O_4/PDMS thin films are expected to have a very important influence on their electrical properties. Sheet resistance measurements of the fabricated samples are presented in Fig. 8. As a general behaviour, the resistance of the irradiated material decreases with the number of accumulated pulses. This resistance reduction is more significant at higher laser

fluences due to the larger modification of the material. The initial sheet resistance of raw GO/PDMS films is about 300 MΩ sq^{-1} (Fig. 8a). The irradiation at 100 mJ cm^{-2} fluence enables its sudden decrease even with low number of accumulated pulses, reaching a resistance of about 5 kΩ sq^{-1} (vacuum) and 3 kΩ sq^{-1} (NH_3), ~5 orders of magnitude lower than that of raw GO/PDMS, after applying 1000 subsequent pulses. Probably, the slightly lower resistance of the films obtained in NH_3 ambient are related to the higher reduction degree of rGO in addition to the presence of pyridinic N in its structure [42,51]. On the other hand, raw GO-Fe_3O_4/PDMS films, due to the presence of interpenetrated insulating oxide NPs and higher oxidation degree than raw GO/PDMS, show a larger sheet resistance of around 600 MΩ sq^{-1} (Fig. 8b). Similarly to GO/PDMS films, the laser irradiation of the GO-Fe_3O_4 composite leads to a substantial decrease of the sheet resistance up to 13 kΩ sq^{-1} and 45 kΩ sq^{-1} in vacuum and NH_3 environments, respectively, after the accumulation of 1000 laser pulses. Remarkably, a decrease of sheet resistance of around 4 orders of magnitude is obtained after laser processing of GO-Fe_3O_4/PDMS films albeit the final GO degree of reduction is quite different when the process in performed in vacuum or ammonia environment (Fig. 6). These results suggest that other structural factors besides chemical composition would strongly affect the electrical conductivity of the obtained materials. In particular, the influence of structural defects and wrinkles on the electrical conductivity of graphene-based materials is revealed to be a key factor. It is widely accepted that structural defects and ripples in graphene material induce electron scattering mechanisms leading to the increase of electrical resistance [52]. Nevertheless, and in contrast to expectation, the obtained results clearly show that the resistivity of the laser irradiated GO/PDMS and GO-Fe_3O_4/PDMS composite films decrease with the accumulation of laser pulses even though the concentration of defects and rippling highly increases (Figs. 2, 3 and 8).

These results are unprecedented and clearly indicate that ultraviolet laser-induced structural and chemical modifications play a complex role in the final sheet resistance of the generated materials. It should be noted that similar behaviour was observed in a previous work by Jafri et al. [53] where the increase of vacancy defects in graphene, obtained by chemical treatment, led to the significant increase of its electrical conductivity. In this case, the effect was attributed to the defect-induced creation of metallic-like regions around the vacancy defects. Further investigations will be focused on the study of the causes of the observed resistance diminishing, as well as the optimization of the applied laser-based processing methods for the development of composite materials with electrical characteristics suitable for future applications.

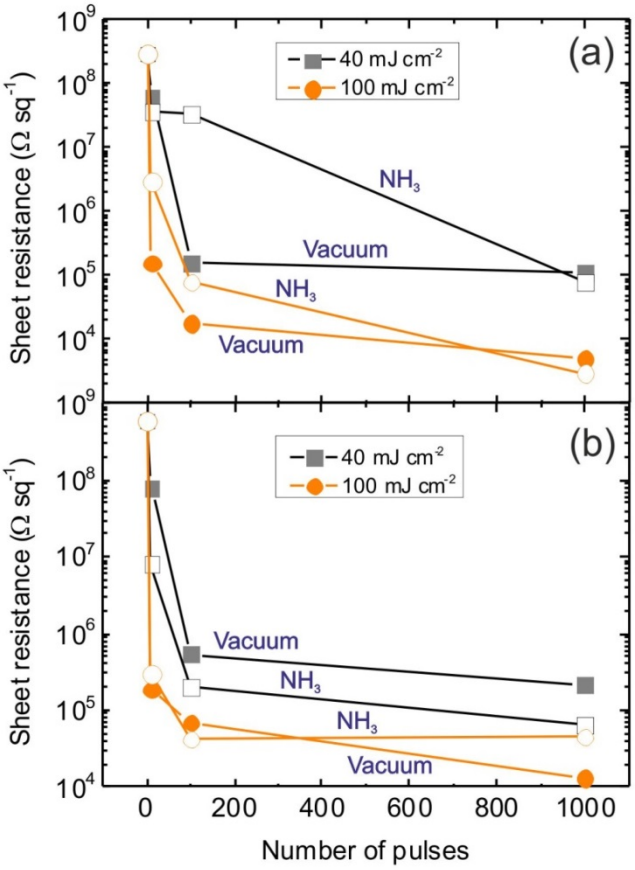

Fig. 8. Sheet resistance of the obtained (a) GO/PDMS and (b) GO-Fe_3O_4/PDMS films.

4. Conclusion

Lightweight GO/PDMS and GO-Fe_3O_4/PDMS films have been obtained in a simple and versatile way. Laser irradiation of these systems leads to a rich variety of structural and chemical modifications which are greatly depending on the environmental conditions. Thus, the build-up of filament-like corrugations in the GO sheets, attributed to the creation of defects and thermomechanical stress in GO, is observed after the accumulation of laser pulses. The irradiation of GO/PDMS films mainly provokes its simultaneous photoreduction, with removal yield distinctive on the oxygen-containing group, and the transformation of amine to pyridinic N-O chemical groups both in vacuum and ammonia-rich environments. In the latter case, the formation of pyridinic nitrogen moieties in the basal plane of rGO structure is also observed. The presence of Fe_3O_4 nanoparticles in GO-Fe_3O_4/PDMS nanocomposite films completely modify the chemical pathway observed in irradiated GO/PDMS. Raw GO-Fe_3O_4/PDMS systems show a slightly oxidized nature of GO. Further laser irradiation induces the reduction of initial GO and the transformation of pyridinic N-O to amine groups, and probably to graphitic nitrogen in ammonia ambient. Interestingly, the sheet resistance of the obtained films decreases as the accumulation of laser pulses proceeds, independently on their chemical composition and increasing concentration of structural defects. The obtained results open a new window for the study of new and adaptable strategies for the development of functional rGO-oxide NPs nanocomposites and their chemical functionalization.

Acknowledgements

The authors acknowledge the financial support of the Spanish Ministry of Economy and Competitiveness under the project ENE2014-56109-C3-3-R, in addition to the Executive Unit for Financing Higher Education, Research, Development, and Innovation of the Romanian Ministry of Education, Research, Youth, and Sports under the Grant PN-II-PT-PCCA-2011-3.2-1235. This work was also performed, in part, at the Center for Integrated Nanotechnologies, an Office of Science User Facility operated for the U.S. Department of Energy (DOE) Office of Science. Los Alamos National Laboratory, an affirmative action equal opportunity employer, is operated by Los Alamos National Security, LLC, for the National Nuclear Security Administration of the U.S. Department of Energy under contract DE-AC52-06NA25396. Wei Gao thanks the start-up funding support from the College of Textiles at North Carolina State University. Josep Puigmarti Luis also acknowledge the Ramon y Cajal program (RYC-2011-08071) from the Spanish Ministry of Economy and Competitiveness.

References

[1] K. Krishnamoorthy, R. Mohan and S. J. Kim. Graphene oxide as a photocatalytic material. Appl. Phys. Lett., 2011, 98, 244101.

[2] D. R. Dreyer, S. Park, C. W. Bielawski and R. S. Ruoff. The chemistry of graphene oxide. Chem. Soc. Rev., 2010, 39, 228-40.

[3] H. C. Hsu, I. Shown, H. Y. Wei, Y. C. Chang, H. Y. Du, Y. G. Lin, et al. Graphene oxide as a promising photocatalyst for CO_2 to methanol conversion. Nanoscale, 2013, 5, 262-68.

[4] Z. S. Wu, G. Zhou, L. C. Yin, W. Ren, F. Li and H. M. Cheng. Graphene/metaloxide composite electrode materials for energy storage. Nano Energy, 2012, 1, 107-31.

[5] X. An and J. C. Yu. Graphene-based photocatalytic composites. RSC Advances, 2011, 1, 1426-34.

[6] F. Meng, J. Li, S. K. Cushing, J. Bright, M. Zhi, J. D. Rowley, et al. Photocatalytic Water Oxidation by Hematite/Reduced Graphene Oxide Composites. ACS Catal,. 2013, 3, 746-51.

[7] T. Wang, Z. Liu, M. Lu, B. Wen, Q. Ouyang, Y. Chen, et al. Graphene–Fe_3O_4 nanohybrids: Synthesis and excellent electromagnetic absorption properties. J. Appl. Phys., 2013,113, 024314.

[8] H. Zhang, A. Xie, C. Wang, H. Wang, Y. Shen and X. Tian. Room temperature fabrication of an RGO–Fe_3O_4 composite hydrogel and its excellent wave absorption properties. RSC Adv., 2014, 4, 14441.

[9] Y. Qin, M. Long, B.Tan and B. Zhou. RhB Adsorption Performance of Magnetic Adsorbent Fe_3O_4/RGO Composite and Its Regeneration through A Fenton-like Reaction. Nano-Micro Lett., 2014, 6, 125-35.

[10] J. Qian, X. Yang, L. Jiang, C. Zhu, H. Mao and K. Wang. Facile preparation of Fe_3O_4 nanospheres/reduced graphene oxide nanocomposites with high peroxidase-like activity for sensitive and selective colorimetric detection of acetylcholine. Sensors Actuat B-Chem., 2014, 201, 160-6.

[11] G. Zhou, D. W. Wang, F. Li, L. Zhang, N. Li, Z. S. Wu, et al. Cheng. Graphene-Wrapped Fe_3O_4 Anode Material with Improved Reversible Capacity and Cyclic Stability for Lithium Ion Batteries. Chem. Mater., 2010, 22, 5306-13.

[12] M. Liu and J. Sun. In situ growth of monodisperse Fe_3O_4 nanoparticles on graphene as flexible paper for supercapacitor. J. Mater. Chem. A, 2014, 2, 12068-74.

[13] T. Chen and L. Dai. Flexible supercapacitors based on carbon nanomaterials. J. Mater. Chem. A, 2014, 2, 10756.

[14] T. F. Yeh , C. Y. Teng, S. J. Chen and H. Teng. Nitrogen-Doped Graphene Oxide Quantum Dots as Photocatalysts for Overall Water-Splitting under Visible Light Illumination. Adv. Mater., 2014, 26, 3297-3303.

[15] L. Li, Y. Dou, L. Wang, M. Luo and J. Liang. One-step synthesis of high-quality N-doped graphene/Fe_3O_4 hybrid nanocomposite and its improved supercapacitor performances. RSC Adv., 2014, 4, 25658-65.

[16] Z. S. Wu, S. Yang, Y. Sun, K. Parvez, X. Feng and K, Müllen. 3D Nitrogen-Doped Graphene Aerogel-Supported Fe_3O_4 Nanoparticles as Efficient Electrocatalysts for the Oxygen Reduction Reaction. J. Am. Chem. Soc., 2012, 134, 9082-5.

[17] Y. Li, Y. Zhao, H. Cheng, Y. Hu, G. Shi, L. Dai and L. Qu. Nitrogen-Doped Graphene Quantum Dots with Oxygen-Rich Functional Groups. J. Am. Chem. Soc., 2012, 134, 15-8.

[18] V. Chandra, J. Park, Y. Chun, J. W. Lee, I. C. Hwang and K. S. Kim. Water-Dispersible Magnetite-Reduced Graphene Oxide Composites for Arsenic Removal. ACS Nano, 2010, 4, 3979-86.

[19] Yi Zhang, B. Chen, L. Zhang, J. Huang, F. Chen, Z. Yang, et al. Controlled assembly of Fe_3O_4 magnetic nanoparticles on graphene oxide. Nanoscale, 2011, 3, 1446-50.

[20] E. György, A. Pérez del Pino, C. Logofatu, A. Duta and L. Isac. Effect of nitrogen doping on wetting and photoactive properties of laser processed zinc oxide-graphene oxide nanocomposite layers. J. Appl. Phys., 2014, 116, 024906.

[21] E. György, A. Pérez del Pino, C. Logofatu, C. Cazan and A. Duta. Simultaneous Laser-Induced Reduction and Nitrogen Doping of Graphene Oxide in Titanium Oxide/Graphene Oxide Composites. J. Am. Ceram. Soc., 2014, 97, 2718-24.

[22] S. M. O'Malley, J. Tomko, A. Pérez del Pino, C. Logofatu and E. György. Resonant Infrared and Ultraviolet Matrix-Assisted Pulsed Laser Evaporation of Titanium Oxide/Graphene Oxide Composites: A Comparative Study. J. Phys. Chem. C, 2014, 118, 27911-9.

[23] G. Graffius, F. Bernardoni and A. Y. Fadeev, Covalent Functionalization of Silica Surface Using "Inert" Poly(dimethylsiloxanes). Langmuir, 2014, 30, 14797–807

[24] A. Pérez del Pino, E. György, C. Logofatu and A. Duta. Study of the deposition of graphene oxide by matrix-assisted pulsed laser evaporation. J. Phys. D Appl. Phys., 2013, 46, 505309.

[25] P. D. Desai. Thermodynamic properties of iron and silicon. J. Phys. Chem. Ref. Data, 1986, 15, 967-83.

[26] T. Nishi, H. Shibata, H. Ohta and Y. Waseda. Thermal Conductivities of Molten Iron, Cobalt, and Nickel by Laser Flash Method. Metall. Mater. Trans. A, 2003, 34A, 2801-7.

[27] A. Schlegel, S. F. Alvarado and P. Wachter. Optical properties of magnetite (Fe_3O_4). J. Phys. C Solid State Phys., 1979, 12, 1157-64.

[28] D. A. Sokolov, C. M. Rouleau, D. B. Geohegan and T. M. Orlando. Excimer laser reduction and patterning of graphite oxide. Carbon, 2013, 53, 81-9.

[29] J. C. Meyer, C. Kisielowski, R. Erni, M. D. Rossell, M. F. Crommie and A. Zettl. Direct Imaging of Lattice Atoms and Topological Defects in Graphene Membranes. Nano Lett., 2008, 8, 3582-6.

[30] L. D. Carr and M. T. Lusk. Graphene gets designer defects. Nat. Nanotechnol., 2010, 5, 316-7.

[31] Z. Qin, M. Taylor, M. Hwang, K. Bertoldi and M. J. Buehler. Effect of Wrinkles on the Surface Area of Graphene: Toward the Design of Nanoelectronics. Nano Lett., 2014, 14, 6520-5.

[32] F. M. Koehler, A. Jacobsen, K. Ensslin, C. Stampfer and W. J. Stark. Selective Chemical Modification of Graphene Surfaces: Distinction Between Single- and Bilayer Graphene. Small, 2010, 6, 1125-30.

[33] C. G. Wang, L. Lan, Y.P. Liu and H.F. Tan. Defect-guided wrinkling in graphene. Comp. Mater. Sci., 2013, 77, 250-3.

[34] C. Wang, Y. Liu, L. Li and H. Tan. Anisotropic thermal conductivity of graphene wrinkles. Nanoscale, 2014, 6, 5703-7.

[35] A. T N'Diaye, R. van Gastel, A. J Martínez-Galera, J. Coraux, H. Hattab, D. Wall, et al. In situ observation of stress relaxation in epitaxial graphene. New J. Phys., 2009, 11, 113056.

[36] A. Pérez del Pino, E. György, L. Cabana, B. Ballesteros and G. Tobias. Ultraviolet pulsed laser irradiation of multi-walled carbon nanotubes in nitrogen atmosphere. J. Appl. Phys., 2014, 115, 093501.

[37] A. M. Alsayed, M. F. Islam, J. Zhang, P. J. Collings and A. G. Yodh. Premelting at Defects Within Bulk Colloidal Crystals. Science, 2005, 309, 1207-10.

[38] S. Seo, Y. Yoon, J. Lee, Y. Park and H. Lee. Nitrogen-Doped Partially Reduced Graphene Oxide Rewritable Nonvolatile Memory. ACS Nano, 2013, 4, 3607-15.

[39] D. A. Sokolov, Y. V. Morozov, M. P. McDonald, F. Vietmeyer, J. H. Hodak and M. Kuno. Direct Observation of Single Layer Graphene Oxide Reduction through Spatially Resolved, Single Sheet Absorption/Emission Microscopy. Nano Lett., 2014, 14, 3172-9.

[40] D. W. Boukhvalov, M. I. Katsnelson. Chemical Functionalization of Graphene with Defects. Nano Lett., 2008, 8, 4373-9.

[41] H. Wang, T. Maiyalagan and X. Wang. Review on Recent Progress in Nitrogen-Doped Graphene: Synthesis, Characterization, and Its Potential Applications. ACS Catal., 2012, 2, 781-94.

[42] B. J. Schultz, R. V. Dennis, J. P. Aldinger, C. Jaye, Xi. Wang, D. A. Fischer, A. N, Cartwright and S. Banerjee. X-ray absorption spectroscopy studies of electronic structure recovery and nitrogen local structure upon thermal reduction of graphene oxide in an ammonia environment. RSC Adv., 2014, 4, 634-44.

[43] T. Xing, Y. Zheng, L. H. Li, B. C. C. Cowie, D. Gunzelmann, S. Z. Qiao, et al. Observation of Active Sites for Oxygen Reduction Reaction on Nitrogen-Doped Multilayer Graphene. ACS Nano, 2014, 8, 6856-62.

[44] T. F.u Yeh, S. J. Chen, C. S. Yeh and H. Teng. Tuning the Electronic Structure of Graphite Oxide through Ammonia Treatment for Photocatalytic Generation of H_2 and O_2 from Water Splitting. J. Phys. Chem. C, 2013, 117, 6516−24.

[45] S. Zhang, X. Zhao, H. Niu, Y. Shi, Y. Cai and G. Jiang. Superparamagnetic Fe_3O_4 nanoparticles as catalysts for the catalytic oxidation of phenolic and aniline compounds. J. Hazard. Mater., 2009, 167, 560-6.

[46] M. Zhu and G. Diao. Synthesis of Porous Fe_3O_4 Nanospheres and Its Application for the Catalytic Degradation of Xylenol Orange. J. Phys. Chem. C, 2011, 115, 18923-34.

[47] E. Antolini. Graphene as a new carbon support for low-temperature fuel cell catalysts. Appl. Catal. B-Environ., 2012, 123– 124, 52-68.

[48] T. Zeng, W. W. Chen, C. M. Cirtiu, A. Moores, G. Song and C. J. Li. Fe_3O_4 nanoparticles: a robust and magnetically recoverable catalyst for three-component coupling of aldehyde, alkyne and amine. Green Chem., 2010, 12, 570-3.

[49] T. Yamashita and P. Hayes. Analysis of XPS spectra of Fe^{2+} and Fe^{3+} ions in oxide materials. Appl. Surf. Sci., 2008, 254, 2441-9.

[50] P. Mills and J. L. Sullivan. A study of the core level electrons in iron and its three oxides by means of X-ray photoelectron spectroscopy. J. Phys. D Appl. Phys., 1983, 16, 723-32.

[51] H. Feng, R. Cheng, X. Zhao, X. Duan and J. Li. A low-temperature method to produce highly reduced graphene oxide. Nat. Comm., 2013, 4, 1539.

[52] A. H. Castro Neto, F. Guinea, N. M. R. Peres, K. S. Novoselov and A. K. Geim. The electronic properties of graphene. Rev. Mod. Phys., 2009, 81, 109-62.

[53] S. H. M. Jafri, K. Carva, E. Widenkvist, T. Blom, B. Sanyal, J. Fransson, et al. Conductivity engineering of graphene by defect formation. J. Phys. D Appl. Phys., 2010, 43, 045404.